Supplementary Information

Differentially photo-crosslinked polymers enable self-assembling microfluidics

Mustapha Jamal[1], Aasiyeh M. Zarafshar[1] and David H. Gracias[1,2]

[1]Department of Chemical and Biomolecular Engineering, Johns Hopkins University, Baltimore, Maryland 21218, USA
[2]Department of Chemistry, Johns Hopkins University, Baltimore, Maryland 21218, USA

Supplementary Figures

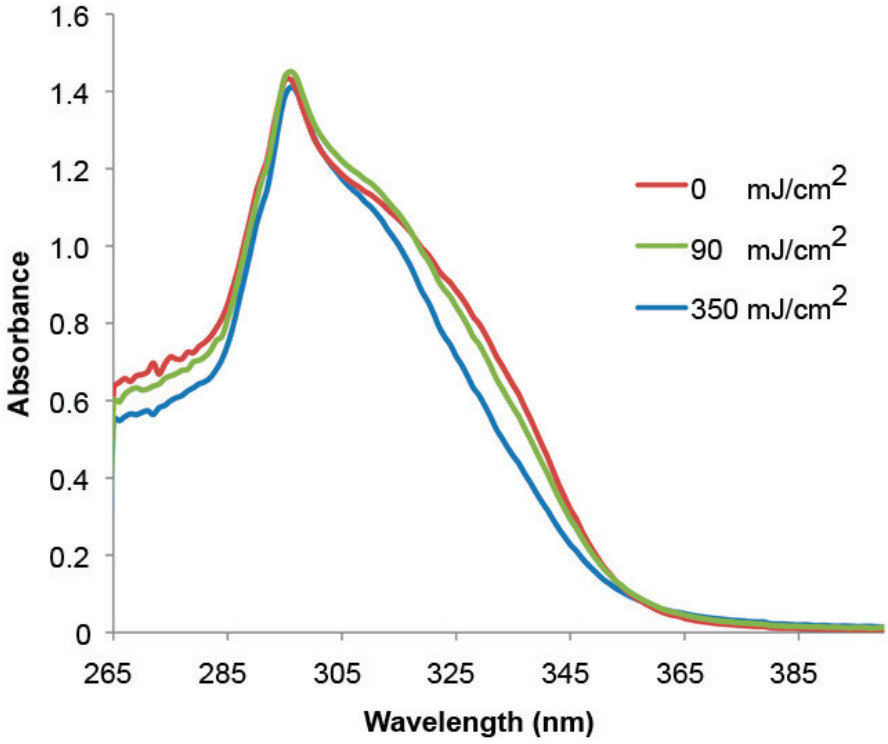

Supplementary Figure S1. Ultraviolet (UV) absorption spectra of 10.7 μm thick SU-8 films. The films were UV-exposed for 0, 90, and 350 mJ/cm^2 prior to taking absorption measurements. The absorption measurements were done using a Spectramax Plus 384 microplate spectrophotometer [Molecular Probes]. The wavelengths were varied in 1 nm intervals and curves represent the average of 4 readings. The measured spectra show that SU-8 absorbs light at low UV wavelengths.

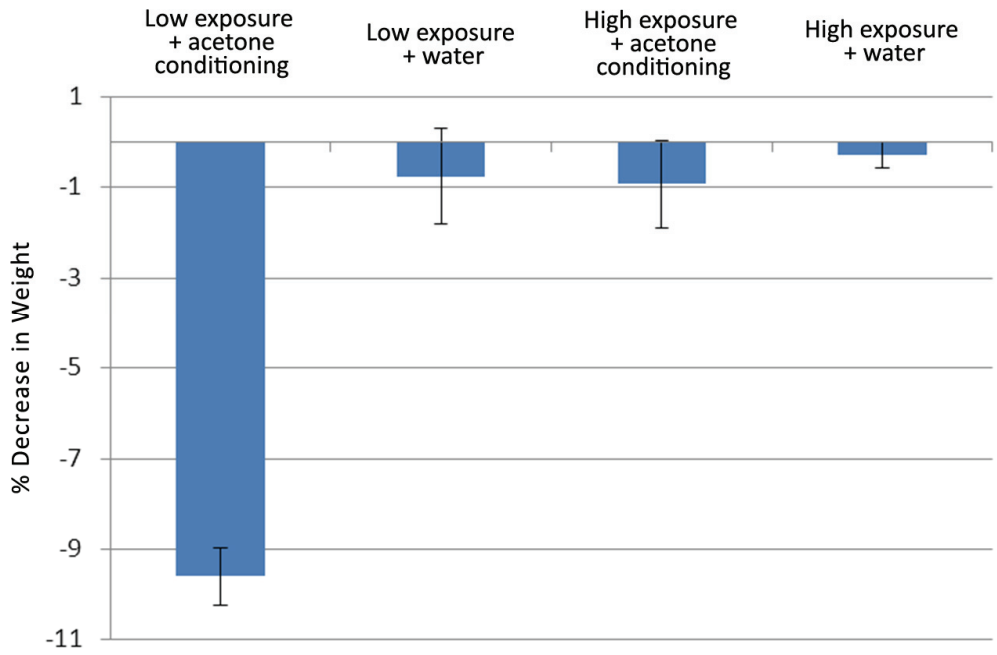

Supplementary Figure S2. Average percentage weight decrease for low- and high-UV exposed SU-8 films that were soaked in either acetone (conditioned) or deionized (DI) water (control). Dry weights were measured before and after the films were soaked. The plotted values represent the average over three samples and the bars denote the standard deviation. A significant dry weight loss of approximately 9.6% was observed for low-UV exposed SU-8 that was acetone conditioned. In contrast, high-UV exposed films that were acetone conditioned, as well as both low and high UV exposed films that were soaked in DI water, showed a weight loss of less than 1%. These results show that acetone conditioning resulted in the removal of un-crosslinked material that was present to a significant extent in low-UV exposed SU-8 films.

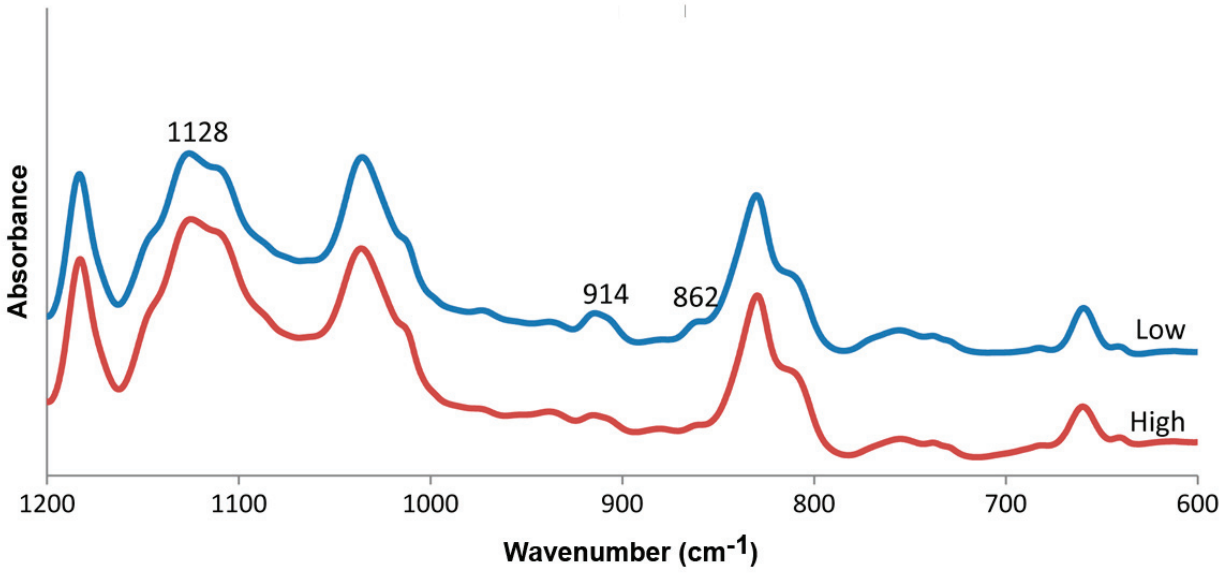

Supplementary Figure S3. FTIR spectra of low- and high-UV exposed SU-8 films prior to acetone conditioning. The high-exposed SU-8 film exhibits a greater peak intensity at 1128 cm^{-1} compared to the low exposed film. This peak is associated with ether bonds of crosslinked SU-8 [ref. 21, 23, main text] and the intensity is expected to increase with increasing crosslinking, as observed. A corresponding decrease in the peak intensities at epoxy group absorbances 914 cm^{-1} and 862 cm^{-1}, associated with epoxide rings of un-crosslinked SU-8 [ref. 21, 23, main text], was also observed for high-exposed SU-8. Both observations confirm that SU-8 is less-crosslinked after low exposures as compared to high exposures, as expected.

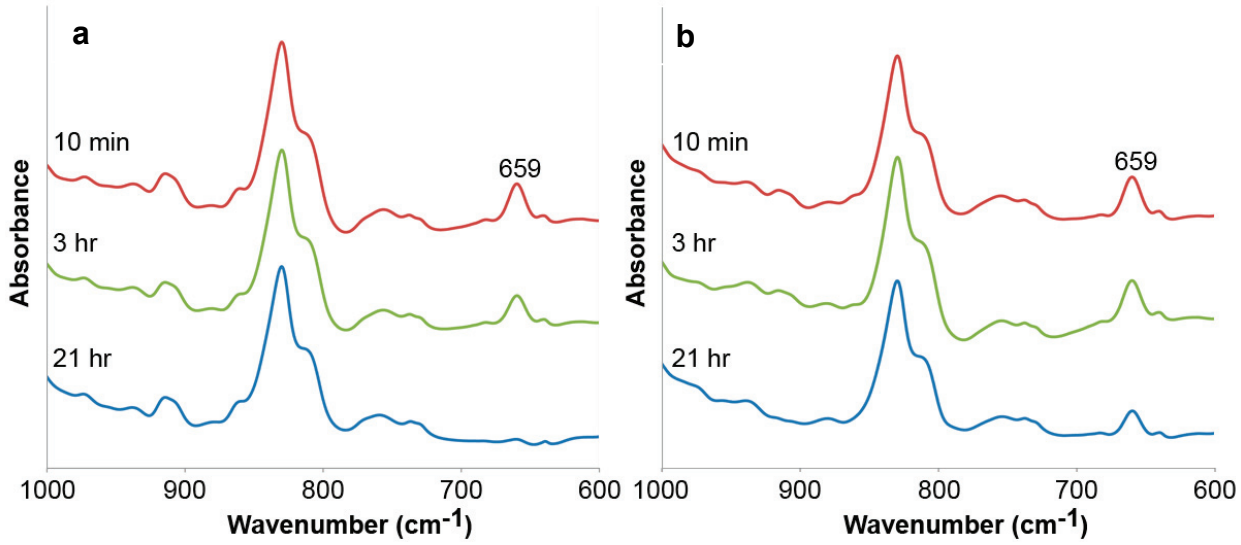

Supplementary Figure S4. FTIR spectra of (**a**) low- and (**b**) high-UV exposed SU-8 films after conditioning in acetone for 10 min, 3 hrs and 21 hrs. All films showed a progressive decrease in absorbance intensity at 659 cm^{-1} with increasing conditioning time. This peak likely corresponds to the photoinitiator triarylsulfonium hexafluoroantimonate [ref. 24, main text] and the decrease in peak height suggests that the photoinitiatior is removed. This removal was dependent on both the extent of crosslinking and the conditioning time. Low-exposed SU-8 films showed a significantly greater and faster decrease in absorbance at this peak.

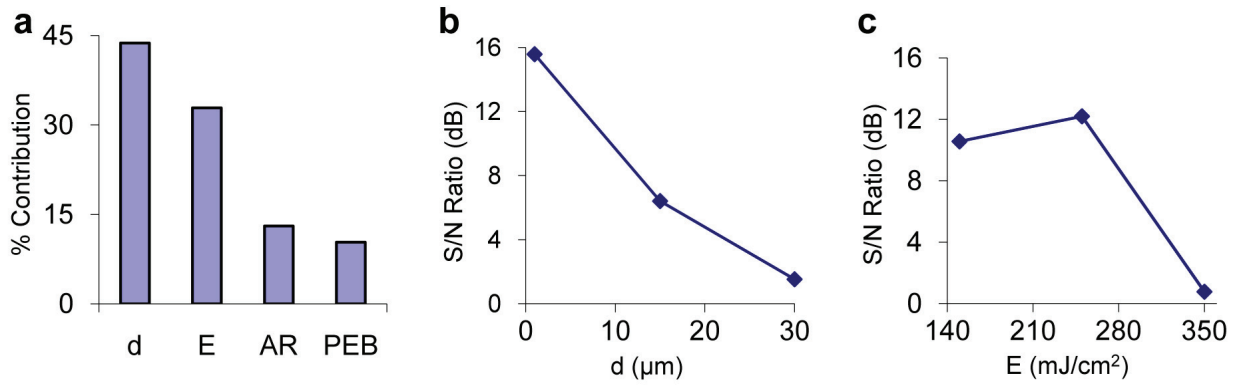

Supplementary Figure S5. a, Percent contribution of individual Taguchi Design of Experiments parameters on SU-8 curvature: d, the film thickness, E, the UV exposure energy, AR, the patterned aspect ratio, and PEB, the post exposure bake temperature. The percent contribution of the different factors was calculated using the analysis of variance statistical method as a part of the Taguchi analysis. SU-8 thickness and UV exposure energy were the two dominant factors, together accounting for 76.5% of the contribution. The post exposure bake temperature and aspect ratio of SU-8 structures were significantly less influential, accounting for 13% and 10%, respectively. **b,** Sensitivity analysis of resist thickness. **c,** Sensitivity analysis of exposure energy.

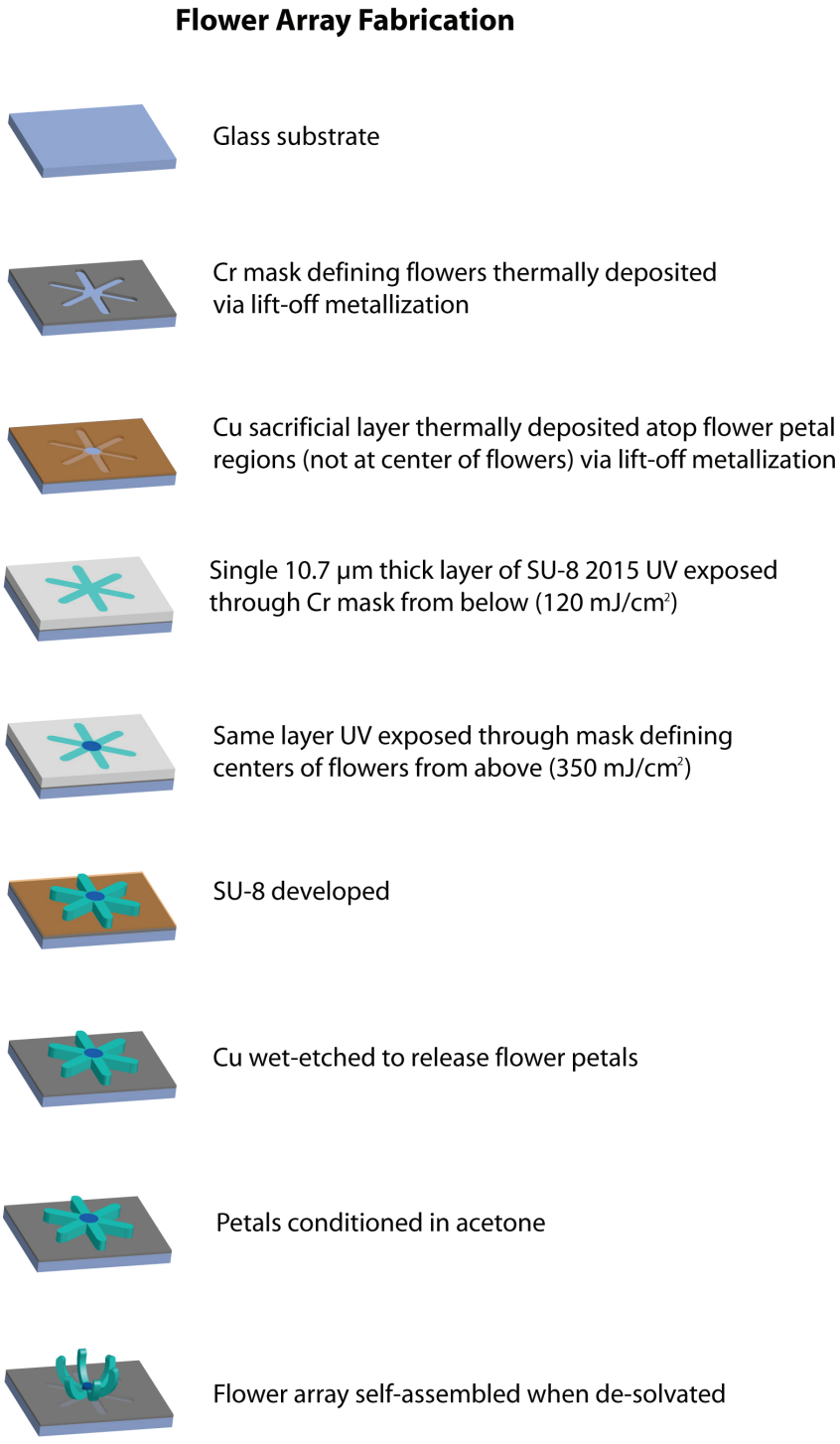

Supplementary Figure S6. Schematic illustration of the fabrication steps for self-assembling flower-shaped structures anchored to a substrate (Fig. 1d, main text).

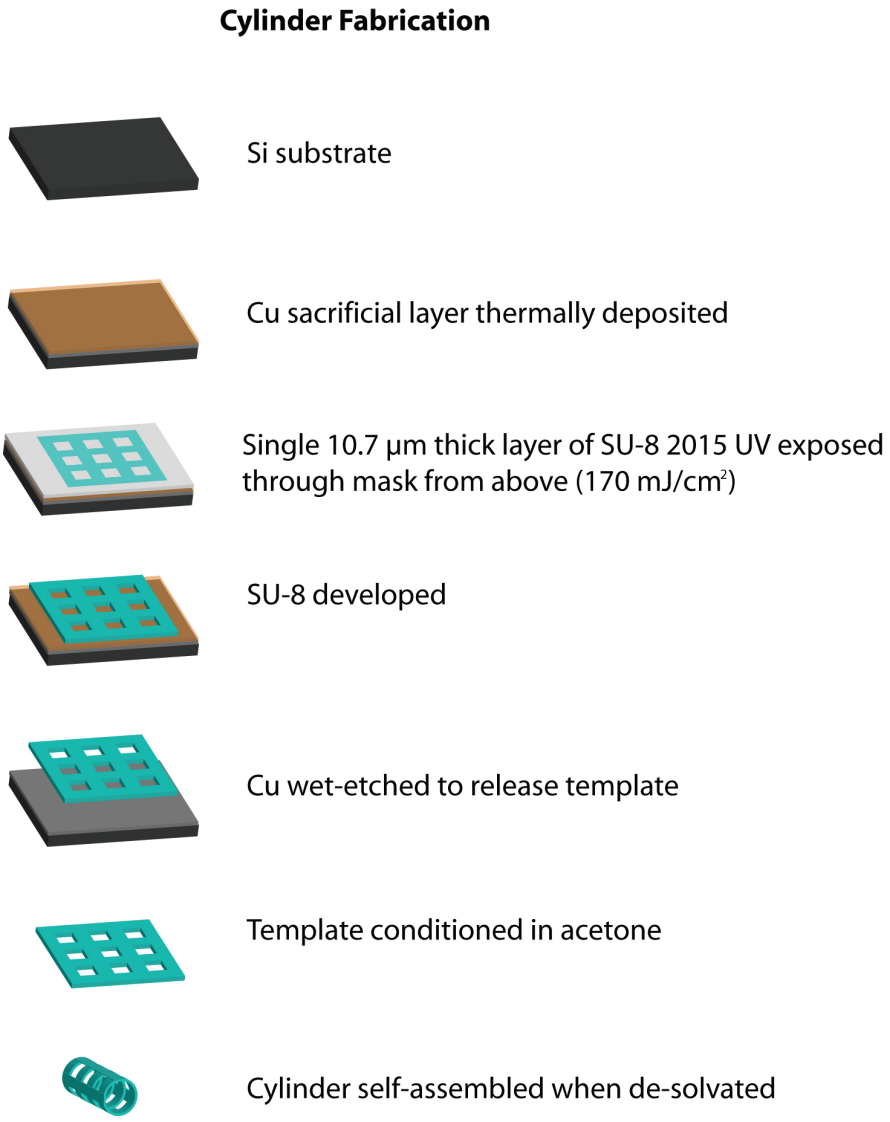

Supplementary Figure S7. Schematic illustration of the fabrication steps for self-assembling cylinders (Fig. 3a, main text).

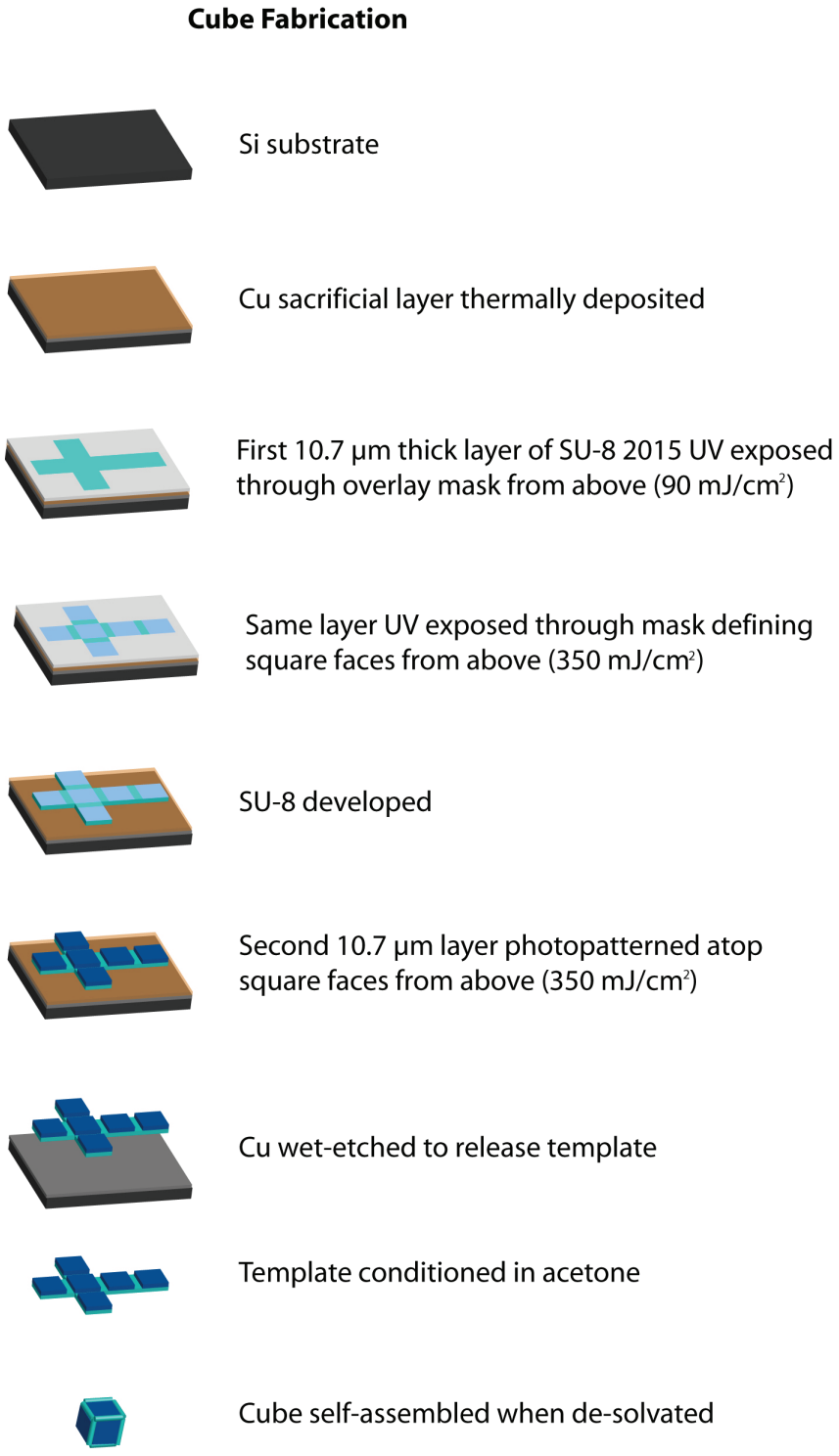

Supplementary Figure S8. Schematic illustration of the fabrication steps for self-assembling cubes (Fig. 3b, main text).

Supplementary Figure S9. Schematic illustration of the fabrication steps for self-assembling bidirectional sheets (Figs. 3c,e,f, main text).

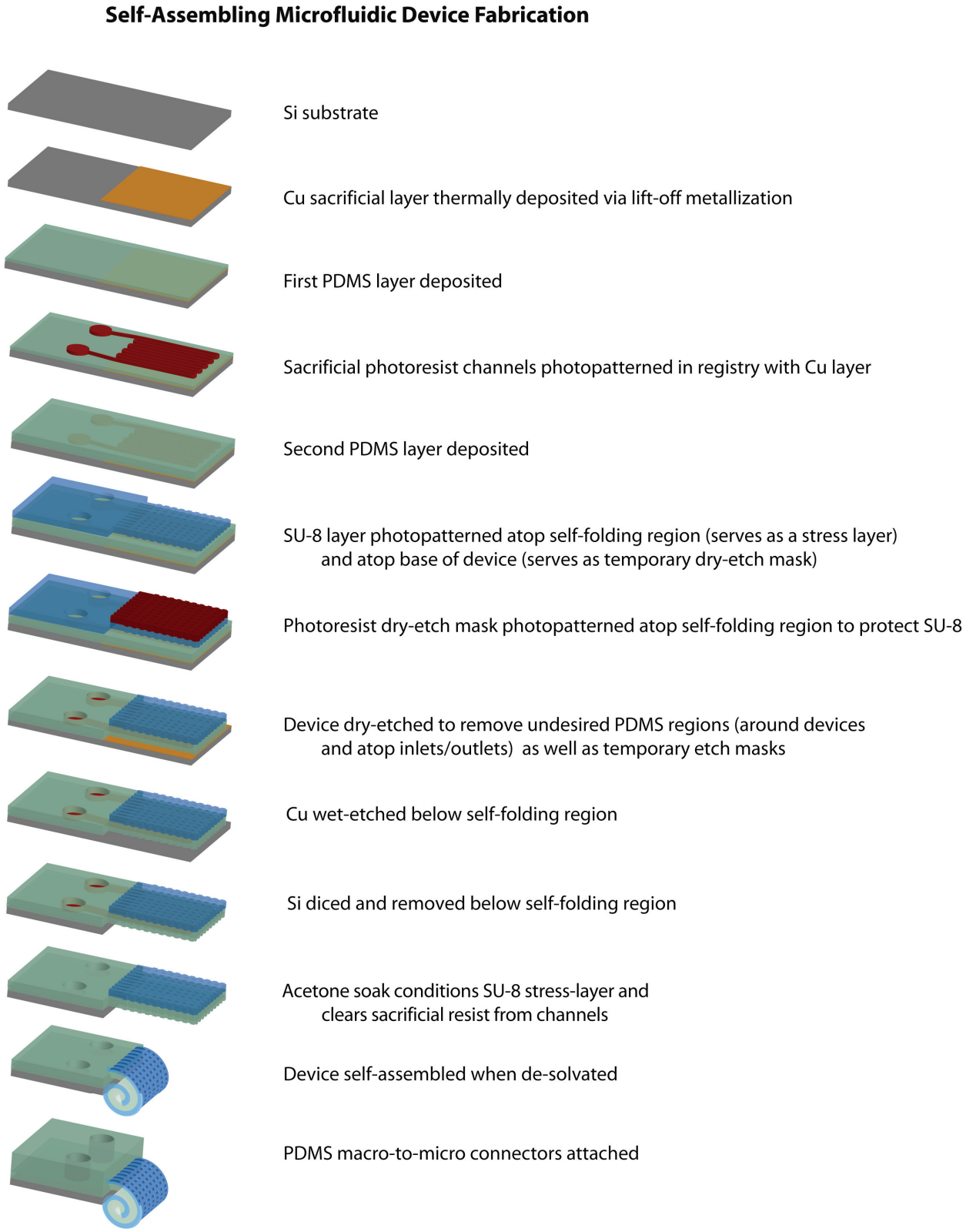

Supplementary Figure S10. Schematic illustration of the fabrication steps for the self-assembling microfluidic devices (Figs. 3d, 4, main text).

Supplementary Tables

TDOE Exp. #	PEB (°C)	UV exposure energy (mJ/cm^2)	Thickness (μm)	Aspect ratio
1	100	150	1	1:1
2	100	250	15	1:6
3	100	350	30	1:30
4	125	150	15	1:30
5	125	250	30	1:1
6	125	350	1	1:6
7	150	150	30	1:6
8	150	250	1	1:30
9	150	350	15	1:1

Supplementary Table S1. Processing parameters for the nine Taguchi experiments.

Exp #	Trial 1	Trial 2	Trial 3	Trial 4	Trial 5	Trial 6	Trial 7	Trial 8	Trial 9	Trial 10	Avg.	S/N ratio
1	17.53	12.80	16.46	13.61	19.86	16.14	16.24	17.83	16.21	15.81	16.25	24.03
2	3.62	3.74	3.70	3.30	3.16	2.77	2.65	2.63	2.59	2.56	3.07	9.46
3	0.91	0.92	0.94	0.94	0.94	1.06	1.03	0.95	0.94	0.93	0.96	-0.42
4	2.38	2.37	2.29	2.29	2.30	2.48	2.24	2.37	2.30	2.38	2.34	7.35
5	1.82	1.81	1.66	1.74	1.59	1.80	1.77	1.62	1.75	1.73	1.73	4.73
6	1.12	0.90	1.82	0.83	0.94	0.92	1.66	1.37	0.77	1.27	1.16	0.31
7	1.07	1.07	1.05	0.94	1.03	1.12	1.05	1.04	0.94	1.06	1.04	0.28
8	9.17	11.31	19.53	18.28	14.92	18.51	11.80	10.43	15.46	15.25	14.47	22.40
9	1.25	1.30	1.27	1.43	1.44	1.41	1.30	1.25	1.26	1.32	1.32	2.39

Supplementary Table S2. Raw and average curvature data obtained in units of mm^{-1} obtained from 10 trials for each of the nine Taguchi experiments.

Film thickness (μm)	SU-8 type	Spin speed (rpm)	Spin ramp duration (sec)	Spin duration (sec)	Soft bake time (min) 75:100:75 ºC	Manufacturer's suggested exposure energy (mJ/cm²)	PEB time (min) 75:100:75 ºC	Development time (min)
1.1	2000.5	300	5	30	1:1:1	102-136	1:1:1	1.00
10.7	2015	5000	5	30	1:3:1	189-251	1:3:1	1.50
14.3	2015	3250	5	30	1:3:1	207-275	1:4:1	1.75
24.0	2015	1430	5	30	1:4:1	223-298	1:5:1	3.00
39.0	2025	2040	5	30	2:6:2	239-319	1:6:1	4.50
50.8	2025	1440	5	30	3:9:3	241-322	2:6:2	5.00

Supplementary Table S3. Processing parameters for SU-8 films of varying thickness. The exposure energies noted in this table represent the range for manufacturer's recommended exposures[40,41] for films photopatterned atop Cu substrates.

Supplementary Note 1

Optical absorption and beam mechanics model relating UV exposure to radius of curvature

Our assumptions are intended to simplify the analysis while providing insight. SU-8 photo-polymerization occurs via acid-initiated cationic polymerization on exposure to UV light. At low exposures, we assume that we are within the energy range where the extent of crosslinking increases linearly with exposure energy [ref. 19, main text]. At high exposures, the extent of cross-linking becomes much less dependent on variations in exposure energies as SU-8 films approach complete crosslinking.

We exposed SU-8 films to UV light using a standard mercury lamp in a commercial mask aligner. In our model, we assume that the substrate over which the SU-8 is deposited is non-reflective so that we can ignore back-illumination from the substrate. We note that the optical absorption of SU-8 is significant at wavelengths shorter than approximately 350 nm (Supplementary Fig. S1). Due to this absorption, the manufacturer recommends the use of an optical filter to cut-off wavelengths below 350 nm during exposure to achieve more uniform SU-8 crosslinking and to enable the patterning of SU-8 structures with straight side-walls[40,41]. It is important to note that we used the multi-band exposure of a mercury UV lamp without the use of filters; hence, we have significant absorption along the thickness of the exposed film at low UV wavelengths. This absorption causes the light intensity at these low wavelengths to decay along the thickness of the film and is pronounced for low-exposed films.

Using the exponential decay of light through an absorbing medium we can write,

$$I_{Bottom} = I_{Top}\exp(-\alpha d) \Rightarrow I_{Top} - I_{Bottom} = I_{Top}\left[1-\exp(-\alpha d)\right] \quad \text{(S1)}$$

where I_{Bottom} and I_{Top} are the intensities of light at the bottom and top sides of the film, α is a constant which depends on the optical absorptivity or attenuation characteristics of SU-8 at a particular wavelength, and d is the thickness of the film.

Due to significant absorption of SU-8 below 350 nm, on low-exposures and in the absence of a filter that would attenuate low wavelength UV absorption, the top part of the film gets exposed more and consequently more crosslinked than the bottom upon post exposure

baking of the film. Thus, a crosslink gradient (CLG) develops. The dependence of this CLG on film thickness and absorptivity can be written as,

$$CLG = \frac{CL_{Top} - CL_{Bottom}}{d} \propto \frac{E_{Top} - E_{Bottom}}{d} \propto E_{Top} \frac{\left[1 - \exp(-\alpha d)\right]}{d} \quad \text{(S2)},$$

so that, $CLG \propto E_{Top} \frac{\left[1 - \exp(-\alpha d)\right]}{d}$ (S3),

where CL is the extent of crosslinking and E is the exposure energy. It should be noted that since we are exposing the films with multi-band exposure, and the absorptivity/photo-crosslinking of SU-8 varies at different wavelengths, it is a first order approximation intended to provide insight into the mechanism. Moreover, this expression is valid only when there is a linear dependence of photo-crosslinking on exposure energies [ref. 19, main text] which we refer to as low-exposure energies.

From equation (S3), we see that at low exposures, the CLG decreases with increasing film thickness, the extent of which depends on the absorptivity. This expression can also be used for other materials and the magnitude of the CLG can be manipulated by altering the film thickness and by using exposures at different wavelengths where the absorptivity varies.

We note that differentially crosslinked films remained flat on release from the substrate. On conditioning the films in acetone, un-crosslinked material is removed resulting in a stress gradient that causes the SU-8 structures to curve on de-solvation. On re-solvation, the gradient is homogenized and the structures flatten out. We characterized the radius of curvature (plotted in Fig. 2b) using rectangular beams of 1.5 mm length, 0.15 mm width and a thickness d ranging from approximately 1 micrometer to 50 micrometers. We note that these structures were rectangular and the thicknesses of the films was much smaller than their lengths (d<<L). Thus, we can utilize rectangular beam bending mechanics[42-44] to relate the radius of curvature R to the stress gradient Γ; $R \propto \frac{1}{\Gamma}$ (S4). Since the stress gradient is derived from the removal of un-crosslinked material from films with a CLG, and the extent of removal is dependent on the extent of crosslinking, we assume that the stress gradient increases with increasing CLG. This assumption is corroborated by all experiments in this paper. The exact relationship between the stress gradient and the CLG depends on other processing factors too, such as acetone

conditioning time. Assuming a linear dependence, $\Gamma \propto CLG$ (S5), we get a relationship between the radius of curvature and the *CLG* as, $R \propto \frac{1}{CLG}$ (S6), which allows us to explain the trends observed in Fig. 2b. For example, we see that for the same exposure energy, the radius of curvature increases with increasing thickness. This observation is validated from the model since it follows from equation (S3) that an increased thickness *d*, decreases the CLG and from equation (S6) that this decreased CLG will result in an increased radius of curvature. Assuming a Young's modulus for SU-8 of 2 GPa and a Poisson's ratio of 0.2, we can estimate the magnitude of the stress gradient to be in the range of 1-32 MPa/μm depending on the thickness of the film.

Supplementary Methods

Self-assembling microfluidic device fabrication (Figs. 3d, 4, main text)

This section describes the fabrication details of the microfluidic devices shown in Figs. 3d, 4 of the main text (see Supplementary Fig. S10 for a detailed schematic). We note that prior to all UV exposure steps, the UV intensity was measured through a bare glass photomask mount to determine the required exposure times. We also note that all bake steps were carried out using aluminium foil-covered hot plates with the substrate temperature checked using a handheld infrared thermometer.

First, a 3 inch diameter silicon (Si) wafer was cleaned with DI water, acetone, 2-propanol, and then dried with nitrogen (N_2) gas. A copper (Cu) sacrificial layer was then patterned via lift-off metallization. Briefly, a 2.7 μm thick layer of SC1827 photoresist (PR) was deposited and photopatterned as per manufacturer's protocol. Thermal evaporation of 15 nm/90 nm chromium/Cu and subsequent dissolution of the photoresist in acetone resulted in the patterned Cu sacrificial regions.

Next, a layer of polydimethylsiloxane (PDMS) [Sylgard 184 Silicone Elastomer Kit; Dow Corning] was deposited atop the wafer after the PDMS had been mixed and degassed. PDMS of a 1:3 curing agent-to-base weight ratio was deposited by spin-coating (2.5 mL at 2500 rpm for 45 sec) and was baked at 100°C for 2 hrs with a 300°C/hr ramp up and 1 hr ramp down to room temperature, yielding a 12 μm thick layer. The Si wafer was dehydration baked at 150°C for 5 minutes immediately prior to depositing the PDMS. We note that a 1:3 curing agent-to-base weight ratio was used for the first PDMS layer since the sacrificial PR channel layer was susceptible to cracking when baked atop less crosslinked PDMS, likely due to the mismatch in thermal expansion coefficients between PR and less crosslinked PDMS.

After baking, the 1:3 PDMS layer was then oxygen (O_2) plasma cleaned [75 W for 90 sec at 0.300 Torr; Technics PEII-A, 30 kHz RF power]. A 10 μm thick PR layer, later patterned into sacrificial microfluidic channels, was immediately spin-coated (2.5 mL spun at 500 rpm for 1 min) and baked with a procedure we developed that largely eliminated cracking of the PR. Specifically, the wafer was exchanged between a 144°C hotplate for 20 sec and an 88°C hotplate for 20 sec. This exchange was repeated five times in succession, after which the wafer was

gradually cooled to room temperature over 1 hr. The PR layer was then exposed (360 mJ/cm^2) in registry with the sacrificial Cu layer and with the photomask in soft contact with the film (all subsequent UV exposures were performed in hard contact). The PR was then developed for 90 sec with gentle agitation in a bath of 1:5 volume ratio of developer [Microposit 351 Developer; MicroChem Corp.] to DI water, rinsed with DI water and dried with N_2 gas. A foam swab was wet with acetone and gently rubbed along the outer edge of the PDMS side of the wafer to remove the remaining photoresist edgebead.

Next, 1:5 PDMS was degassed, spin-coated (2.5 mL at 2500 rpm) and baked at 85°C for 4 hrs with a 300°C/hr ramp up, followed by a 1 hr ramp down to room temperature, resulting in a 18 μm thick top PDMS layer. This bake was carried out at a lower temperature and longer duration than the previously deposited 1:3 layer in order to sufficiently cure the top PDMS layer yet prevent the underlying PR layer from cracking. We also note that a 1:5 ratio was used for the top PDMS layer since subsequently deposited photoresist materials are not as susceptible to cracking due to thermal expansion of PDMS.

After baking the top PDMS layer, a 25 μm thick layer of SU-8 2015 was patterned in registry with the underlying layers. Briefly, the wafer was first plasma cleaned as before. Next, 2.5 mL of SU-8 2015 was immediately spin-coated at 1600 rpm for 38 sec, soft baked on a hot plate set at 40°C with a 300°C/hr ramp and 15 min hold at 85°C, and then gradually cooled to room temperature over 1 hr. The SU-8 layer was exposed (350 mJ/cm^2) and post exposure baked on a room temperature hotplate ramped to 85°C at 300°C/hr, then immediately set to gradually cool to room temperature over 1 hr. The wafer was developed in SU-8 Developer while stirring at 200 rpm. SU-8 Developer can diffuse through PDMS; hence, prolonged and continuous developments caused the sacrificial PR embedded within the PDMS layers to reflow. Developments were therefore carried out in 30 sec immersions, followed by drying with N_2 gas over 30 sec. The immersion/drying cycle was repeated five times for an overall immersion duration of 2.5 min, after which the wafer was briefly rinsed with acetone and 2-propanol before being dried with N_2 gas.

The unwanted regions of PDMS were removed via a dry-etch step with O_2 and carbon tetrafluoride (CF_4). These regions included macro-to-micro inlets/outlets for pumping fluids through the devices. The previously patterned SU-8 layer served as both a stress layer for the

self-assembling region of the device, and as an etch mask at the inlet/outlet region of the device that remains on the Si substrate ("base of the device"). An NR4-8000P resist layer [Futurrex, Inc.] served as a second etch mask, atop the SU-8 self-assembling region only. Briefly, the wafer was plasma cleaned as before and 2.5 mL of NR4-8000P was immediately spin-coated at 3500 rpm for 40 sec. The wafer was soft baked using a similar procedure as for the sacrificial PR channel layer, but the temperatures were 144°C/91°C with a total resting time of 90 sec at 144°C. This process yielded an 8 μm thick layer of NR4-8000P. Next, the NR4 layer was UV exposed (3000 mJ/cm^2 as measured with a 405 nm wavelength sensor), and then post exposure baked at 85°C for 5 min with a 300°C/hr ramp up followed by a 1 hr ramp down to room temperature. The resist was developed in an RD-6 bath [Futurrex, Inc.] for 195 sec, rinsed with DI water, and dried with N_2 gas. The wafer was then dry-etched using a planar etcher [270 W, 15 sccm CF_4, 5 sccm O_2, and a chamber pressure of 0.250 Torr; PE-100 etcher; Plasma Etch, Inc]. The observed etch rates were approximately 22 μm/hr for PDMS and 15 μm/hr for SU-8/NR4. We conducted preliminary tests using a Technics PEII-A, 30 kHz RF power planar etcher at 300 W with the same gas ratio and measured etch rates of 15 μm/hr for PDMS and 8 μm/hr for SU-8/NR4. The dry-etch step was carried-out until both the bulk PDMS around each device and the SU-8 etch mask atop the base of the devices were completely removed. Thicknesses were measured using a DekTak IIA stylus profilometer.

After dry-etching, the self-assembling SU-8/PDMS portion of the device was released from the underlying Si wafer by selectively dissolving the Cu sacrificial layer in an aqueous etchant composed of 40% ferric chloride and 5% HCl. Using a diamond tipped scribe, the Si substrate was manually diced to separate each of the simultaneously microfabricated devices and to enable the overhanging of the released SU-8/PDMS portion. Removing the released Si substrates below the SU-8/PDMS portions assured the Si would not physically prevent self-assembly of the devices. Next, the devices were immersed in an acetone bath overnight to both condition the SU-8 stress layers and to dissolve the sacrificial PR layers thereby unblocking the embedded channels. The devices self-assembled upon the addition of DI water to the bath and then were dried in air.

Macro-to-micro interfacing with the thin, self-assembled devices was achieved by manually coring PDMS blocks and attaching them to the microfabricated inlets/outlets at the base of the devices[45]. Briefly, 1:10 curing agent-to-base weight ratio PDMS was first poured into

a Petri dish and baked at 60°C for several hours. The PDMS slab was removed and cut into approximately 3 mm by 3 mm by 1 cm blocks, each with a 1 cm long hole punched using a Harris Uni-core puncher to later form tight fits around syringe needles of varying gauge (ex. 0.5 mm punchers for 22 gauge needles). Each connector was placed atop an inlet/outlet using a 3 mm by 3 mm sheet of 50 μm thick double-sided tape [Catalog # SA-S-1L, Grace Bio-Labs] with a 2 mm diameter hole punched through. Once attached to the base of a device, the array of PDMS connecters was surrounded by rigid plastic sides (~15 mm tall), the space around the connectors was filled with 5 minute epoxy, and device fabrication was then complete.

Devices were loaded with fluorescent solutions using a modified vacuum loading protocol[46] and with syringe pumps. Although not required for the channel geometries utilized in our manuscript, the pre-filling of complex microfluidic networks with buffer solution can greatly improve device operation by eliminating the trapping of air bubbles that may otherwise disrupt fluid flow. Vacuum loading (Fig. 4) was achieved by first connecting plastic syringes (with their plungers removed) to 22 gauge blunt needles and then inserting the needles into the PDMS connectors. The syringes were then filled with solutions (1 mM fluorescein or 500 μM rhodamine B in ethanol) and the assemblies were placed in a desiccator for 10 min to remove air from the device channels. Upon releasing the vacuum, the fluorescent solutions filled the channels. Submerging the self-assembled regions of the devices in DI water during loading ensured air did not re-enter the devices through the thin PDMS walls upon release of the vacuum, which would have hampered filling of the channels.

Syringe pumps were also independently utilized to infuse solutions into the devices. Solutions were typically pumped using syringes connected to 24 gauge Teflon tubing. A 22 gauge luer lock needle connected to a syringe was typically insert into one end of a Teflon tube, and a 23 gauge stainless steel cylinder [0.025 inch OD, 0.17 inch ID, 1 inch long; Catalog # NE-1300-02, New England Small Tube] was inserted in the other end of the Teflon tube and then to the PDMS connectors of the devices. Needles could be disconnected/reconnected to the macro-to-micro interface without introducing air bubbles if the head volume above the base of the device (formed by the aforementioned ~15 mm plastic sides) was filled with DI water to prevent the trapping of bubbles at the inlets when syringes were subsequently removed or added.

Imaging equipment and settings

Fluorescence images (Figs. 1d, 3a-d, and 4e,f) were captured using a Nikon AZ100 multi-zoom microscope, a motorized stage for capturing z-stacks, and a Nikon DS-Fi1 camera. Fig. 1d and Fig. 3a-d were captured using a UV-2E/C ultraviolet excitation filter. Fig. 4e was captured using a Nikon B-2E/C blue excitation filter. Fig. 4f was captured using both a Nikon B-2E/C blue excitation filter and a Nikon G-2E/C green excitation filter, one immediately after the other.

Bright field images were captured using either the aforementioned Nikon AZ100 setup (Fig. 3e-inset, Fig. 3f, and Fig. 4c,d) or a Canon Powershot S3 IS camera (Fig. 3e-main image, and Fig. 4b). In particular, the flat structure in Fig. 3e was imaged by first conditioning the film in a Teflon dish containing acetone and subsequently evaporating the acetone at ambient room conditions, which resulted in the structure remaining stuck to the Teflon surface in its flat state. The same exact structure was then re-solvated in acetone to release it from the Teflon surface, de-solvated upon the addition of DI water to self-assemble the structure, and then imaged while submerged in DI water (Fig. 3f-main) and after being dried in air (Fig. 3f-inset).

For all z-stack micrographs, focused images were created using the extended depth of field (EDF) algorithm within Nikon's NIS-Elements software. Image acquisition settings were consistent across the z-stack of each individual sample. Brightness and contrast were linearly adjusted for all micrographs using Adobe Photoshop.

The relative fluorescence line plots presented in Fig. 2a were acquired from fluorescence micrographs of sectioned samples that were sliced using a LEICA Ultracut UCT ultramicrotome (see methods section of the main text) and imaged with a Zeiss Axiovert 200 microscope, Semrock FF409-EM02-25 ultraviolet excitation filter and a Cooke Sensicam camera. The fluorescence micrographs were captured with the software SlideBook using identical acquisition settings. The relative fluorescence line plots were subsequently created by averaging lines from three randomly selected regions of the sections using the software ImageJ.

References

40. SU-8 2000 Permanent Epoxy Negative Photoresist Process Guidelines For: SU-8 2000.5, SU-8 2002, SU-8 2005, SU-8 2007, SU-8 2010 and SU-8 2015 (Ver. 4.0) [Online]. Available: http://www.microchem.com/pdf/SU-82000DataSheet2000_5thru2015Ver4.pdf

41. SU-8 2000 Permanent Epoxy Negative Photoresist Processing Guidelines For: SU-8 2025, SU-8 2035, SU-8 2050 and SU-8 2075 (Ver. 4.0) [Online]. Available: http://www.microchem.com/products/pdf/SU-82000DataSheet2025thru2075Ver4.pdf

42. Gere, J. M. and Timoshenko, S. P., *Mechanics of Materials 4th Ed*. Boston: PWS Pub. Co., 1997.

43. Rebeiz, G. M., *RF MEMS: Theory, Design, and Technology*. New Jersey: John Wiley & Sons, 2003.

44. Chinthakindi, A. K. and Kohl, P. A., Electrostatic actuators with intrinsic stress gradient. *J. Electrochem. Soc.,* **149**, H146-H152 (2002).

45. Mohanty, S. and Beebe, D. J., Chips & Tips: PDMS connectors for macro to microfluidic interfacing. (2006) [Online]. Available: http://www.rsc.org/Publishing/Journals/lc/PDMS_connector.asp

46. Monahan, J. M., Gewirth, A. A., and Nuzzo, R. G., A method for filling complex polymeric microfluidic devices and arrays. *Anal. Chem.***73**, 3193-3197 (2001).